Article

pubs.acs.org/JPCC

Put Your Backbone into It: Excited-State Structural Relaxation of PffBT4T-2DT Conducting Polymer in Solution

- 3 Varuni Dantanarayana, ^{†,||} Jack Fuzell, ^{†,||} Dingqi Nai, [‡] Ian E. Jacobs, [‡] He Yan, [§] Roland Faller, [‡]
- 4 Delmar Larsen, †,*® and Adam J. Moule *,*
- 5 [†]Department of Chemistry, University of California, Davis 95616, United States
- 6 [‡]Department of Chemical Engineering, University of California, Davis 95616, California, United States
- 7 [§]Department of Chemistry and Hong Kong Branch of Chinese National Engineering Research Center for Tissue Restoration and
- s Reconstruction, Hong Kong University of Science and Technology (HKUST), Clear Water Bay, Kowloon, Hong Kong
- 9 Supporting Information

10

11

12

13

14

15

16

17

18

19

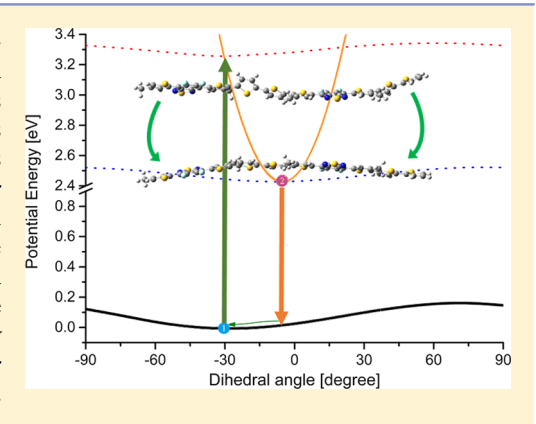
20

2.1

22

23

ABSTRACT: Conformational and energetic disorders in organic semiconductors reduces charge and exciton transport because of the structural defects, thus reducing the efficiency in devices such as organic photovoltaics and organic light-emitting diodes. The main structural heterogeneity is because of the twisting of the polymer backbone that occurs even in polymers that are mostly crystalline. Here, we explore the relationship between polymer backbone twisting and exciton delocalization by means of transient absorption spectroscopy and density functional theory calculations. We study the PfBT4T-2DT polymer which has exhibited even higher device efficiency with nonfullerene acceptors than the current record breaking PCE11 polymer. We determine the driving force for planarization of a polymer chain caused by excitation. The methodology is generally applicable and demonstrates a higher penalty for nonplanar structures in the excited state than in the ground state. This study highlights the morphological and electronic changes in conjugated polymers that are brought about by excitation.



5 INTRODUCTION

26 The primary photodynamics of organic semiconductors 27 (OSCs) has been intensely studied over the last two decades 28 in organic photovoltaics (OPV) and other opto-electronic 29 devices. 1-6 The efficiency of such devices depends on a strong 30 understanding of how material choice and design affect device 31 function. 6-8 Even though conjugated polymers in OSCs have 32 been extensively investigated, the mechanism for efficient 33 exciton transport which is crucial for high device efficiency is 34 still not properly understood. Conformational and energetic 35 disorder in conjugated polymers reduces charge-transport 36 efficiency by providing energetic traps that localize the charge 37 carriers because of extensive heterogeneity. A main source of this heterogeneity is the twisting of polymer backbones around 39 rotatable bonds between planar building blocks which occurs 40 even in polymers that are mostly crystalline. 9,10 Thus, exploring 41 the relationship between exciton delocalization and the 42 behavior of the polymer backbone structure in picoseconds 43 after excitation of a polymer is of particular interest.

Previously, 11 we studied the photophysics of the conjugated 45 polymer poly(3-hexylthiophene-2,5-diyl) (P3HT) in solution. 46 We found that coiled P3HT planarizes rapidly (~2 ps) upon 47 excitation. The timescale for returning to a coiled state after 48 return to the ground state was an order of magnitude greater 49 (~20 ps). This planarization of the polymer backbone in the

excited state was monitored by observing the red shift of the 50 stimulated emission (SE) as a function of time after the 51 excitation pulse in a transient absorption (TA) spectroscopy 52 experiment. Other groups have observed excited-state planarization in numerous other conjugated polymers using ultrafast 54 spectroscopy. 411–20 We now quantify the driving force for the 55 planarization of a conjugated polymer chain in the presence of 56 an exciton

PffBT4T-2DT (Figure 1a) was selected for our case study 58 f1 because of the large changes in the ground-state delocalization 59 as a function of dihedral disorder along the polymer 60 backbone. PffBT4T-2DT has the same backbone structure, 61 but longer alkyl chains and less crystallinity than poly[(5,6-62 difluoro-2,1,3-benzothiadiazol-4,7-diyl)-alt-(3,3-di(2-octyldo-63 decyl)-2,2'; 5',2"; 5",2"' -quaterthiophen-5,5-diyl)] (PffBT4T-64 2OD), the OPV record-breaking polymer discovered by Yan et 65 al. PffBT4T-2DT has been shown to deliver even higher OPV 66 efficiency with nonfullerene acceptors than PffBT4T-2OD 67 (PCE11). Here, we demonstrate that the excited-state 68 dynamics of the polymer in solution gives a reasonably simple 69

Received: February 7, 2018 Revised: February 22, 2018 Published: February 23, 2018 The Journal of Physical Chemistry C

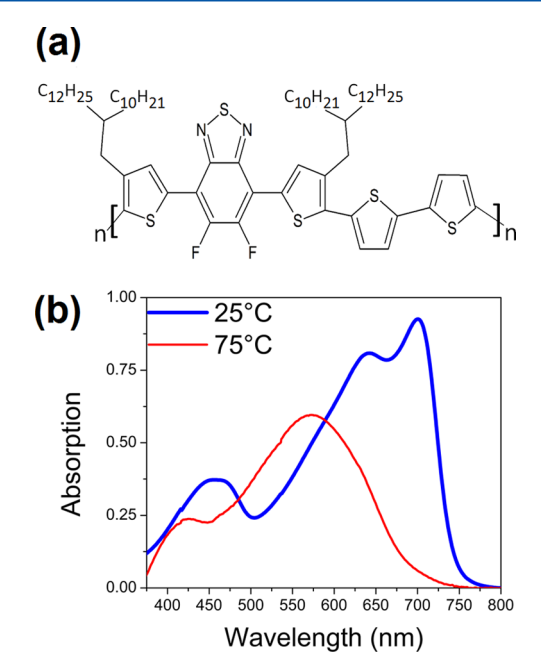


Figure 1. (a) Chemical structure of PffBT4T-2DT and (b) static spectra of PffBT4T-2DT at 25 °C (blue) and 75 °C (red).

70 probe of the coupling between the exciton and structural order 71 in a conjugated polymer.

We present the first full TA spectroscopy data of pure 73 PffBT4T-2DT in solution at two temperatures, 25 and 75 °C, 74 with an excitation wavelength of 400 nm and a broadband 75 probe that covers the visible and near IR spectrum. To interpret 76 these TA spectroscopy data, we use ab initio density functional 77 theory (DFT)^{23,24} to calculate the ground-state energy 78 manifold as a function of dihedral angle rotation along the 79 polymer backbone as well as time-dependent DFT (TD-80 DFT)²⁵ to calculate the excited-state energy as a function of the 81 polymer configuration for both coiled and relaxed (planar) 82 geometries of a PffBT4T-2DT dimer. Not many comparisons 83 between excited-state DFT and TD-DFT calculations on 84 conjugated polymers have been presented previously. 26-28 85 Here, we calculate and discuss the accurate way of computing 86 the molecular geometries and electronic energies involved in a 87 vertical excitation under a rigid rotational scan and use these 88 calculations to develop structurally sensitive potential energy 89 landscapes for both ground and excited states.

90 EXPERIMENTAL AND COMPUTATIONAL 91 METHODS

Spectroscopy. The PffBT4T-2DT sample was dissolved in dichlorobenzene, and TA signals were collected in experiments at 25 and 75 °C. The temperature measurements were performed starting with low temperatures on the same day in back-to-back measurements. For the temperature control, the PffBT4T-2DT sample was kept at 25 and 75 °C using a Fisher Scientific Isotemp 1016D recirculating heat bath and a homemade glass sample holder. Before the data were collected, the sample was circulated at the set temperature for 15 min to ensure equilibration. The PffBT4T-2DT samples were excited with 400 nm pulses created by doubling the fundamental output of our Spectra-Physics Spitfire titanium sapphire laser. The probe pulse was formed by focusing the 800 nm fundamental pulses into a slowly moving 2 mm calcium fundamental pulses into a slowly moving 2 mm calcium fundamental fundamental pulses were collected with a 256 pixel silicon

array. The evolution-associated difference spectra (EADS) were 107 calculated using CarpetView spectroscopy data analysis 108 software.

Computational Methods. DFT calculations were per- 110 formed on the PffBT4T dimer in vacuum. Bulky alkyl chains 111 are mainly used as a solubilizing group in PffBT4T-2DT²⁹ 112 substituted with methyl groups for computational economy. 113 The optimized geometries and the energies were calculated 114 using the Gaussian 09 package.³⁰ The structures were fully 115 optimized in the ground-state and first-excited-state energies at 116 the 6-311G(d,p) basis set level. The subsequent potential 117 energy calculations in ground-state calculations were performed 118 with the 6-31G/B3LYP functional (the Becke 3 and the Lee- 119 Yang-Parr hybrid functional) and the lowest excited singlet 120 state with the TD-DFT approach and 6-31G/CAM-B3LYP 121 functional (B3LYP with Coulomb attenuating method).³¹ This 122 particular basis set was chosen as a compromise between high 123 computational cost and quality of the theoretical calculation. 124 The long-range Coulomb-attenuated B3LYP functional, CAM- 125 B3LYP, has proven to be more accurate when predicting 126 excited-state energies.³² Furthermore, a rigid potential energy 127 surface (PES) around the dihedral angle with the lowest 128 torsional energy was calculated to get the vertical excitation 129 energy to the first-excited singlet state. We realize that even 130 though there are effects (e.g., polymer molecular weight, longer 131 alkyl chain substituent, level of theory, solvent effects, and 132 temperature effects) which tend to affect the exact energy levels 133 that are not considered in these theoretical calculations, it is 134 possible to obtain valuable information by comparing 135 calculations of the same or similar types.

■ RESULTS AND DISCUSSION

Ground-State Spectra and Polymer Conformation. 138 Many thiophene-based conjugated systems exhibit large 139 solvochromic and thermochromic shifts associated with the 140 dihedral disorder along the polymer backbone. 33 PffBT4T-2DT 141 also shows strong thermochromism in solution; therefore, 142 varying the solution temperature affects the aggregation and 143 backbone structure. We use the solution temperature to control 144 the polymer configuration and then probe the ultrafast 145 photodynamics of aggregated and unaggregated morphologies. 146 The static absorption spectra of PffBT4T-2DT at 25 °C (blue 147 curve) and 75 °C (red curve) are compared in Figure 1b. Both 148 of the static spectra match the temperature-dependent static 149 spectra reported previously for PffBT4T-2OD.²¹ The vibronic 150 peaks at 650 and 700 nm in the 25 °C spectrum show³⁴ that 151 PffBT4T-2DT forms aggregates of planar chains, allowing 152 strong delocalization of the ground-state wave function along 153 the backbone. According to the Spano model, 35 the presence of 154 J-aggregate characteristics indicates that individual polymer 155 chains are highly planar with weak intermolecular coupling 156 between chains. This means that at 25 °C, the PffBT4T-2DT 157 chain is constrained to be planar but that the ground-state wave 158 function is not delocalized across multiple chains. The polymer 159 can be treated as a single planar molecule. At 75 $^{\circ}\text{C}\text{,}$ the 160 absorption spectrum exhibits broad peaks centered at 410 and 161 560 nm, corresponding to high structural heterogeneity and 162 localized ground-state wave functions. This verifies that at 163 higher temperatures, the polymers in solution are single-coiled 164 chains which disrupts the conjugation along the polymer 165 backbone.²¹ Thus, the polymer strands are less constrained and 166 more mobile, which allows for the polymer strand to change its 167 conformation when excited and minimizing its free energy.

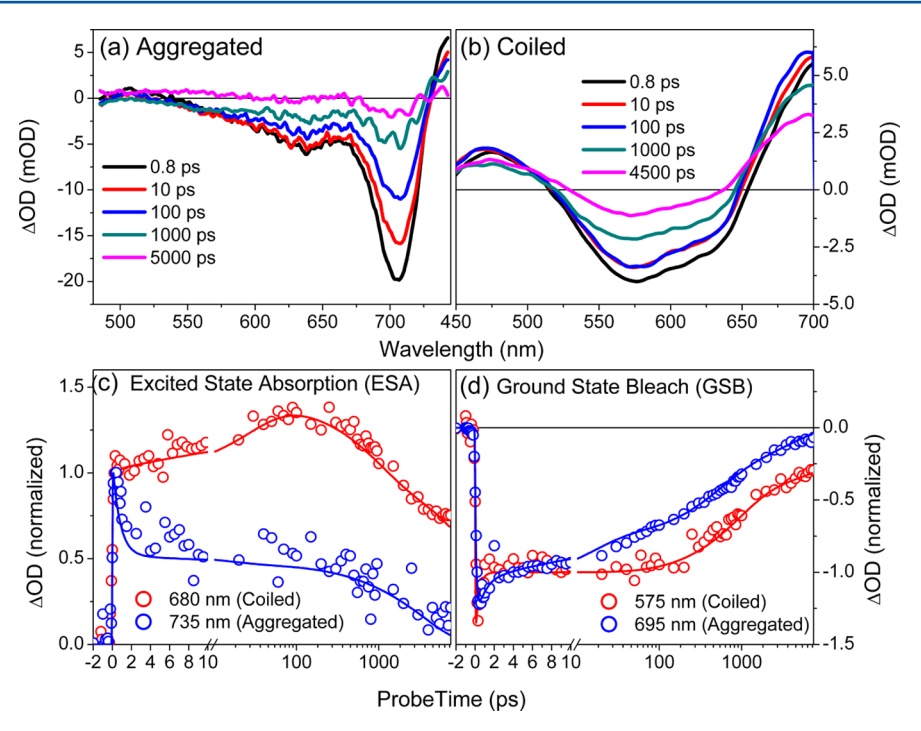


Figure 2. TA spectra at selected time points after 400 nm excitation for both (a) 25 °C (aggregated) and (b) 75 °C (coiled). Note the different spectral windows between the two panels. Kinetics showing (c) ESA and (d) GSB of PffBT4T-2DT at 25 °C (aggregated) and 75 °C (coiled). Note, in the kinetic plots, the linear to logarithmic transition in the plots at 10 ps.

TA Spectroscopy and Excited-State Dynamics. Figure 2a,b shows TA spectra of PffBT4T-2DT dissolved in chlorobenzene at 25 and 75 °C, respectively. Both sets of spectra are dominated by the ground-state bleach (GSB), the large negative signal from ~525 to ~725 nm in the 25 °C sample and from ~510 to ~650 nm in the 75 °C sample that represent the depopulation of the ground state by the excitation pulse. Positive excited-state absorption (ESA) bands are located on the red side at >725 nm in the aggregated 25 °C sample and at >650 nm in the coiled 75 °C sample. Furthermore, there are additional ESA bands on the blue side of the spectra with peaks at 510 nm in the 25 °C sample and at 475 nm in the 75 °C sample. The 75 °C solution excited-state bands are blue-shifted 182 compared to the 25 °C solution (Figure 2), similar to their 183 respective spectral features in the ground-state spectra (Figure 184 1b). This blue-shifting can be attributed to polymer strands being less aggregated in the 75 °C sample. In Figure 2a,b, the blue and red ESA bands exhibit near identical decay kinetics (Supporting Information Figure S1), which indicate that we only have one visible, initially excited-state population at each temperature. Given that there is no spectral evolution of either 190 ESA in the first few picoseconds, they must represent the spectral signature of the singlet exciton in PffBT4T-2DT. 13 If the excited polymer does form polarons, they occur faster than our temporal resolution (\approx 100 fs). In comparison with other polymers in solution (e.g., P3HT), 11 PffBT4T-2DT does not exhibit clear SE near its primary absorption band in either the 25 °C or the 75 °C solution.

The excited-state kinetics is strongly dependent on the polymer configuration. For the solutions at both temperatures, the excited-state kinetics (Figure 2c,d) was fit using multi-wavelength global analysis. The kinetic data for each solution were fit using a set of four EADS (Supporting Information Figure S2): EADS are fixed spectra that evolve into each other on certain time scales to fit the data, where each of the fixed

EADS corresponds to the TA spectrum of the raw data in the 204 given time frame. Ignoring the early time (<1 ps) decay because 205 of exciton annihilation caused by the high-incident fluence of 206 the excitation pulse, the GSB (Figure 2d) is flat for ≈100 ps 207 before the decay back to the ground state begins in the coiled 208 75 °C sample (red curve), whereas decay of the GSB to the 209 ground state begins immediately in the aggregated 25 °C 210 sample (blue curve). This is due to the difference in localization 211 effects as seen in other polymers: 5,37,38 localized excitons move 212 by hopping and are slower than delocalized excitons that can 213 sample larger regions of the polymer and begin to decay almost 214 immediately. The longest decay constant in the 25 °C solution 215 is 3.6 ns (blue curve in Figure 2d), whereas the longest decay 216 constant in the 75 °C solution (red curve in Figure 2d) cannot 217 be determined because of the time range of our experimental 218 setup (>7.5 ns).

The two solutions differ in another important way: both ESA 220 and GSB for the aggregated 25 $^{\circ}$ C solution (blue curve in 221 Figure 2c,d, respectively) decay monotonically, whereas in the 222 coiled 75 $^{\circ}$ C solution (red curve in Figure 2c,d, respectively) 223 the absorption on the red side of Figure 2b (\simeq 630 to >700 nm) 224 shows an increase in the signal on a 30 ps time scale. This 225 secondary increase is attributed to a spectral blue shift of the 226 ESA peak in the 75 $^{\circ}$ C sample.

Previously, when we measured P3HT in methanol where the 228 SE red-shifts on a 2 ps timescale, 11 it was attributed to the 229 planarization of the polymer backbone in the excited state. 230 Other thiophene-based polymers, such as oligothiophenes 231 and poly[3-(2,5-dioctylp-henyl)thiophene], 232 exhibit similar 232 behavior on comparable time scales, 46 and 15 ps, respectively. 233 Thus, we attribute this spectral shift to the planarization of the 234 PffBT4T-2DT backbone in the excited state. Although SE 235 shifting is generally used to identify backbone planarization in 236 TA spectroscopy measurements, 11 we do not observe SE over 237 our measured wavelength because of an overlapping ESA band. 238

The Journal of Physical Chemistry C

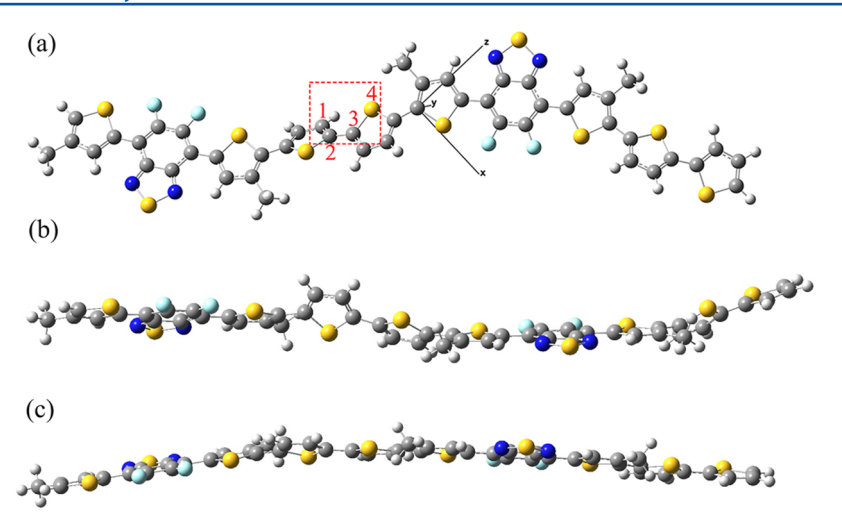


Figure 3. (a) Molecular geometry of the optimized structure of the PffBT4T-2DT dimer. Labeled atoms in the red box denote the dihedral angle around which the rigid rotational PES is calculated. Side views of the optimized geometry of the (b) ground state and (c) first excited state of the PffBT4T-2DT dimer. Color scheme: gray C atoms, yellow S atoms, teal F atoms, blue N atoms, and white H atoms.

239 Instead, we utilize the blue-shifting of the peak of the red-side 240 ESA. This absorption band blue-shifts because the occupied 241 excited-state energy level relaxes, increasing the gap between 242 itself and the higher-lying unoccupied excited states. It is 243 possible for intersystem crossing (ISC) to occur in conjugated 244 polymers and for triplet excitons to form on this 30 ps time 245 scale. However, if singlet excitons were transitioning to triplet 246 excitons, there would be a decrease in the initially populated 247 ESA bands, which we do not observe.

Other options for describing the ~33 ps spectrum blue shift 249 in the 75 °C sample are triplet exciton formation or some form 250 of excited-state charge transfer. Generally, the charge transfer in polymer carries with it a signature in the NIR spectrum, 252 where multiple states with different decay rates will be 253 visible. 40,41 In our data (Supporting Information Figure S3), 254 the NIR spectra do not show multiple populations as the entire 255 spectrum decays with the same time constants (Supporting 256 Information Figure S2). Therefore it seems that the charge 257 transfer is not a good explanation. As the sample was not 258 measured both with and without O2, we are not able to rule out 259 definitively that the spectral blue shift is caused by triplet 260 exciton formation. However, we do not believe this to be the 261 case because both the formation time (~33 ps) and the decay 262 time (nanosecond scale) are too fast in general to be ascribed 263 to triplet excitons. As triplet excitons that form through ISC in polymers such as P3HT or PTB7 form on the nanosecond 265 timescale 40,42 and they decay on the microsecond timescale, not 266 the nanosecond timescale that we observe for the resulting excited state after the blueshift. 43,44

Simulating Excited-State Energies and Conformations. We performed a full geometry optimization on a
model PffBT4T dimer (Figure 3a) in two different energy
configurations. We replaced the full C₂₄H₄₉ side chain in
pffBT4T-2DT by a methyl group for the computational
efficiency. The ground-state geometry was optimized using
DFT/B3LYP⁴⁵ (Figure 3b) and the first excited-singlet-state
geometry (Figure 3c) using TD-DFT/CAM-B3LYP³¹ (see the
supporting Information for computational details). All
simulations were performed with Gaussian 0930 using the 6simulations were performed with Gaussian 0930 using the 6structures that the lowest energy configuration for the ground
state exhibits variations of the dihedral angles (Table S1) along

the backbone, whereas the lowest energy structure in the 281 excited state is planar (Figure 3a,b, respectively), similar to 282 P3HT in solution¹¹ The fluorine atoms reduce the torsional 283 angle of the polymer backbone because of the high electron- 284 withdrawing capability of fluorine and strong attraction 285 between the fluorine and sulfur on the adjacent thiophene. 46 286 We observe that the backbone is flat on either side of the 287 fluorine-substituted benzothiadiazole unit in, both, the ground 288 and the first excited states. The alkyl side chains, in contrast, 289 tend to cause an increase in the dihedral disorder of the 290 polymer backbone.⁴⁷ A systematic study of side chain 291 branching shows that branching at the C2 position combined 292 with long side chains leads to thin-film polymers with low 293 dihedral disorder and high charge mobilities as exhibited in 294 PffBT4T-2DT. 48,49 We can infer that if our PffBT4T model 295 included longer alkyl chain substituents, then the dihedral 296 angles would be even more coiled in the ground state than that 297 found here. Additionally, from the bond-length analysis 298 (Supporting Information Table S2), we see that the PffBT4T 299 dimer exhibits shorter single bonds and longer double bonds 300 along the conjugated backbone upon excitation, corresponding 301 to stronger conjugation than that in the ground state. This is a 302 strong indication for higher-charge delocalization in the first 303 excited state.

To identify which backbone dihedral has the lowest rotation 305 barrier in solution, we calculated the rotational potential energy 306 around each of the nine dihedral angles along the dimer 307 backbone (Supporting Information Figure S3). The calcu- 308 lations were performed by rotating each dihedral by a small 309 angle in both directions from the equilibrium ground-state 310 geometry and then computing the average energy for each 311 dihedral angle. The dihedral angle that is easiest to rotate 312 (lowest torsional potential) is between the two unsubstituted 313 thiophene rings depicted by a red box in Figure 3a. The 314 subsequent detailed rigid torsional potential calculations were, 315 for computational efficiency, performed exclusively around this 316 angle, using the 6-31G basis set at the level of theory 317 mentioned above.

We calculated the excitation energy ($\Delta E_{\rm vert}$) for each ground- 319 state configuration as a function of the dihedral angle around 320 this easiest-to-rotate bond. We performed rigid rotational scans, 321 that is, calculated the single-point energies for every 15° of 322

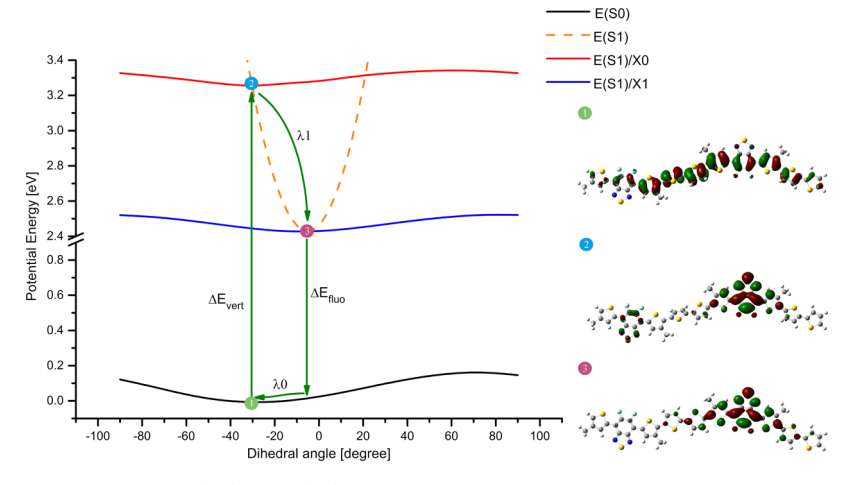


Figure 4. Rotational PESs for PffBT4T dimer. E(S0) and E(S1)/X0 depict the ground-state and excited-state energies, respectively, in the ground-state optimized geometry, whereas E(S1)/X1 is the excited-state energy around the optimized excited-state geometry. The dashed line E(S1) indicates the excited-state energy curve, after instantaneous vertical excitation from the ground-state optimized geometry (point 1 to point 2) and fast relaxation to point 3 within the excited-state energy manifold. Contour plots of the molecular orbitals for the ground-state HOMO energy and excited-state LUMO energy, respectively, in the optimized ground-state geometry (points 1 and 2) and optimized excited-state LUMO energy level (point 3).

323 rotation around the dihedral angle covering the range of -90° 324 to $+90^{\circ}$ while maintaining all other bond lengths and angles at 325 the values of the equilibrium geometry. These vertical 326 transitions are depicted in Figure 4. Although this calculation 327 does not reproduce the full ground-state PES, it introduces 328 significant structural disorder and allows understanding of the 329 effect of dihedral disorder on the excited-state relaxation 330 dynamics.

The vertical transition represented by $\Delta E_{\rm vert}$ (point (1) to 332 (2) in Figure 4) corresponds to the instantaneous electronic 333 charge transfer while the nuclei are still in their ground-state 334 geometry. Thus

$$\Delta E_{\text{vert}} = E(S1, X0) - E(S0)$$

335 where E(S0) (Figure 4 black curve) is the ground-state energy 336 and E(S1,X0) (Figure 4 red curve) is the first singlet-excited-337 state energy at the ground-state equilibrium geometry, X0. 338 After the vertical transition to the excited state, the molecule 339 will rapidly relax to the energy-minimized excited-state 340 geometry, X1, depicted as point (3) Figure 4. This excited-341 state relaxation is driven by the reorganization energy (point 342 (2) to (3) in Figure 4)

$$\lambda 1 = E(S1, X0) - E(S1, X1)$$

343 and follows the pathway shown by the potential energy curve 344 labeled E(S1) under harmonic approximation in Figure 4. 345 We calculated E(S1,X0) (Figure 4 red curve) and E(S1,X1)

We calculated E(S1,X0) (Figure 4 red curve) and E(S1,X1) 346 (Figure 4 blue curve) by determining the excited-state energy at 347 the ground-state equilibrium geometry and excited-state 348 equilibrium geometry, respectively, as a function of the rigid 349 rotation around the easiest-to-rotate dihedral in Figure 3a 350 around the minimized geometry of the excited state. E(S1) 351 (Figure 4 dashed line) represents the excited-state energy 352 surface, which encompasses the electronic energy change and 353 nuclear rearrangement. This curve was obtained by coupling 354 the vertical transition point and excited state minimum after 355 structural relaxation. Naturally, a different E(S1) exists for each 356 ground-state configuration where each E(S1) relaxes to the 357 same X1 configuration.

Similarly, fluorescence from the excited state to the ground 358 state corresponds to 359

$$\Delta E_{\text{fluo}} = E(S1, X1) - E(S0, X1)$$

Finally, the molecule can relax back to the ground-state 360 minimized geometry with reorganization energy 361

$$\lambda 0 = E(S0, X1) - E(S0, X0)$$

The molecular orbital contour plots for E(S0), E(S1,X1), and $^{362}E(S1,X1)$ are depicted in Figure 4. The electron density 363 transfers from E(S0) highest occupied molecular orbital 364 (HOMO) to E(S1,X0) lowest unoccupied molecular orbital 365 (LUMO) in the $E_{\rm vert}$ transition. Clearly, the E(S1,X0) wave 366 function is strongly localized because of the dihedral disorder in 367 the polymer backbone. When E(S1,X0) relaxes to E(S1,X1) 368 LUMO, the dihedral disorder is removed and the wave function 369 delocalizes over more polymer subunits.

This series of calculations shows that $\lambda 1 \gg \lambda 0$ for all 371 molecular configurations, which is why the excited-state 372 relaxation is rapid and the ground-state relaxation is 373 comparatively slow. It can be observed that although the 374 excited-state PES (S1) shows a deep well (Figure 4 dashed 375 line), the ground-state energy profile (S0) is quite flat, 376 indicating that the molecule in its planar excited state is 377 significantly stiffer than in the coiled ground state. We posit 378 that $\lambda 1$ will be much larger than $\lambda 0$ for all conjugated polymers 379 in solution and that the experimental and theoretical method- 380 ology presented here constitutes a systematic way to compare 381 the effect of molecular geometry on the excited-state 382 reorganization energy in conjugated polymers.

CONCLUSIONS

In conclusion, ultrafast TA spectroscopy was performed on 385 PffBT4T-2DT solutions at 25 and 75 °C corresponding to 386 planar and coiled backbone configurations. In addition, the 387 ground-state DFT and excited-state TD-DFT calculations were 388 carried out on the ground-state and first-singlet excited-state of 389 the PffBT4T-2DT dimer. The TA spectroscopy data showed 390 that at 25 °C, the sample has a predominantly planar 391 aggregated polymer configuration even in the ground state. 392

393 The exciton is immediately delocalized without the need for 394 relaxation of the polymer chain to a planar configuration. Thus, 395 the decay back to the ground state starts right away. In 396 comparison, at 75 °C, the polymer is in a coiled unaggregated 397 state and has a localized exciton. To minimize the energy of the 398 exciton, the polymer chain quickly relaxes to a planar 399 configuration, which delocalizes the exciton causing its ESA 400 to blue shift. Once the polymer is locally planarized, the exciton 401 decays to the ground state. The kinetics of the coiled polymer 402 showed that they planarize in the excited state on the 403 picosecond timescale. This interpretation was supported by 404 the DFT and TD-DFT calculations where we found that the 405 PffBT4T-2DT dimer is coiled in the ground state and becomes 406 planar and exhibits a higher degree of conjugation in its first-407 singlet excited state. Within the Franck-Condon principle, we 408 have accurately calculated the excited state energy along with 409 the geometrical changes. In addition, we showed that the 410 excited-state relaxation energy is, in general, much higher than 411 the ground-state relaxation energy and thereby provides a 412 driving force for planarization in the excited state because of the 413 presence of the exciton. The calculation of this driving force 414 over a variety of configurations suggests that the energetic 415 driving force to planarize the polymer backbone in the excited 416 state is a general feature of the conjugated polymers.

417 ASSOCIATED CONTENT

8 Supporting Information

The Supporting Information is available free of charge on the ACS Publications website at DOI: 10.1021/acs.jpcc.8b01356.

Decay kinetics, difference spectra, TA spectra, DFT optimized geometry parameters, DFT calculated torsion potential, and Mulliken charges (PDF)

24 AUTHOR INFORMATION

425 Corresponding Authors

426 *E-mail: dlarsen@ucdavis.edu. Phone: +1 (530) 204-8319 427 (D.L.).

428 *E-mail: amoule@ucdavis.edu. Phone: +1 (530) 754-8669

429 (A.J.M.).

421

422

423

430 ORCID ©

431 Ian E. Jacobs: 0000-0002-1535-4608

432 He Yan: 0000-0003-1780-8308

433 Roland Faller: 0000-0001-9946-3846

434 Delmar Larsen: 0000-0003-4522-2689

435 Author Contributions

436 V.D. and J.F. contributed equally to this work.

437 Notes

438 The authors declare no competing financial interest.

39 ACKNOWLEDGMENTS

440 This project was carried out with funding from the U.S. 441 Department of Energy, Office of Basic Energy Sciences, 442 Division of Materials Sciences and Engineering, under Award 443 DE-SC0010419 to AM and from the National Science 444 Foundation (DMR-1035468) to DSL. We thank the Hong 445 Kong Innovation and Technology Commission for support 446 through projects ITC-CNERC14SC01 and ITS/083/15.

147 REFERENCES

448 (1) Facchetti, A. π-Conjugated Polymers for Organic Electronics and 449 Photovoltaic Cell Applications. *Chem. Mater.* **2011**, *23*, 733–758.

- (2) Burroughes, J. H.; Bradley, D. D. C.; Brown, A. R.; Marks, R. N.; 450 Mackay, K.; Friend, R. H.; Burns, P. L.; Holmes, A. B. Light-emitting 451 Diodes Based on Conjugated Polymers. *Nature* **1990**, 347, 539–541. 452
- (3) Friend, R. H.; Gymer, R. W.; Holmes, A. B.; Burroughes, J. H.; 453 Marks, R. N.; Taliani, C.; Bradley, D. D. C.; Santos, D. A. D.; Brédas, J. 454 L.; Lögdlund, M.; et al. Electroluminescence in Conjugated Polymers. 455 Nature 1999, 397, 121.
- (4) Tretiak, S.; Saxena, A.; Martin, R. L.; Bishop, A. R. 457 Conformational Dynamics of Photoexcited Conjugated Molecules. 458 *Phys. Rev. Lett.* **2002**, *89*, 097402.
- (5) Kaake, L. G.; Moses, D.; Heeger, A. J. Coherence and 460 Uncertainty in Nanostructured Organic Photovoltaics. *J. Phys. Chem.* 461 Lett. 2013, 4, 2264–2268.
- (6) Xin, G.; Baumgarten, M.; Müllen, K. Designing π-Conjugated 463 Polymers for Organic Electronics. *Prog. Polym. Sci.* **2013**, 38, 1832–464 1908
- (7) Vogelbaum, H. S.; Sauvé, G. Recently Developed High-Efficiency 466 Organic Photoactive Materials for Printable Photovoltaic Cells: A Mini 467 Review. *Synth. Met.* **2017**, 223, 107–121.
- (8) Arias, A. C.; MacKenzie, J. D.; McCulloch, I.; Rivnay, J.; Salleo, A. 469 Materials and Applications for Large Area Electronics: Solution-Based 470 Approaches. *Chem. Rev.* **2010**, *110*, 3–24.
- (9) Venkateshvaran, D.; Nikolka, M.; Sadhanala, A.; Lemaur, V.; 472 Zelazny, M.; Kepa, M.; Hurhangee, M.; Kronemeijer, A. J.; Pecunia, V.; 473 Nasrallah, I.; et al. Approaching Disorder-Free Transport in High- 474 Mobility Conjugated Polymers. *Nature* **2014**, *515*, 384–388.
- (10) Korovyanko, O. J.; Österbacka, R.; Jiang, X. M.; Vardeny, Z. V.; 476 Janssen, R. A. J. Photoexcitation Dynamics in Regioregular and 477 Regiorandom Polythiophene Films. *Phys. Rev. B: Condens. Matter* 478 *Mater. Phys.* **2001**, 64, 235122.
- (11) Busby, E.; Carroll, E. C.; Chinn, E. M.; Chang, L.; Moulé, A. J.; 480 Larsen, D. S. Excited-State Self-Trapping and Ground-State Relaxation 481 Dynamics in Poly(3-hexylthiophene) Resolved with Broadband 482 Pump–Dump–Probe Spectroscopy. J. Phys. Chem. Lett. 2011, 2, 483 2764–2769.
- (12) Park, K. H.; Kim, P.; Kim, W.; Shimizu, H.; Han, M.; Sim, E.; 485 Iyoda, M.; Kim, D. Excited-State Dynamic Planarization of Cyclic 486 Oligothiophenes in the Vicinity of a Ring-to-Linear Excitonic 487 Behavioral Turning Point. *Angew. Chem., Int. Ed. Engl.* **2015**, *54*, 488 12711–12715.
- (13) Guo, J.; Ohkita, H.; Benten, H.; Ito, S. Near-IR Femtosecond 490 Transient Absorption Spectroscopy of Ultrafast Polaron and Triplet 491 Exciton Formation in Polythiophene Films with Different Regior- 492 egularities. J. Am. Chem. Soc. 2009, 131, 16869–16880.
- (14) Kim, P.; Park, K. H.; Kim, W.; Tamachi, T.; Iyoda, M.; Kim, D. 494 Relationship between Dynamic Planarization Processes and Exciton 495 Delocalization in Cyclic Oligothiophenes. *J. Phys. Chem. Lett.* **2015**, *6*, 496 451–456.
- (15) Gallaher, J. K.; Chen, K.; Huff, G. S.; Prasad, S. K. K.; Gordon, 498 K. C.; Hodgkiss, J. M. Evolution of Nonmirror Image Fluorescence 499 Spectra in Conjugated Polymers and Oligomers. *J. Phys. Chem. Lett.* 500 **2016**, 7, 3307–3312.
- (16) Yu, W.; Donohoo-Vallett, P. J.; Zhou, J.; Bragg, A. E. Ultrafast 502 Photo-Induced Nuclear Relaxation of a Conformationally Disordered 503 Conjugated Polymer Probed with Transient Absorption and Femto-504 second Stimulated Raman Spectroscopies. J. Chem. Phys. 2014, 141, 505 044201.
- (17) Yu, W.; Zhou, J.; Bragg, A. E. Exciton Conformational Dynamics 507 of Poly(3-hexylthiophene) (P3HT) in Solution from Time-Resolved 508 Resonant-Raman Spectroscopy. *J. Phys. Chem. Lett.* **2012**, *3*, 1321–509
- (18) Zhou, J.; Yu, W.; Bragg, A. E. Structural Relaxation of 511 Photoexcited Quaterthiophenes Probed with Vibrational Specificity. *J.* 512 Phys. Chem. Lett. **2015**, *6*, 3496–3502.
- (19) Chang, M.-H.; Hoffmann, M.; Anderson, H. L.; Herz, L. M. 514 Dynamics of Excited-State Conformational Relaxation and Electronic 515 Delocalization in Conjugated Porphyrin Oligomers. *J. Am. Chem. Soc.* 516 **2008**, *130*, 10171–10178.

The Journal of Physical Chemistry C

- 518 (20) Parkinson, P.; Müller, C.; Stingelin, N.; Johnston, M. B.; Herz, 519 L. M. Role of Ultrafast Torsional Relaxation in the Emission from
- 520 Polythiophene Aggregates. J. Phys. Chem. Lett. 2010, 1, 2788–2792.
- (21) Liu, Y.; Zhao, J.; Li, Z.; Mu, C.; Ma, W.; Hu, H.; Jiang, K.; Lin,
- 522 H.; Ade, H.; Yan, H. Aggregation and Morphology Control Enables 523 Multiple Cases of High-Efficiency Polymer Solar Cells. *Nat. Commun.* 524 **2014**. 5, 5293.
- 525 (22) Li, Z.; Jiang, K.; Yang, G.; Lai, J. Y. L.; Ma, T.; Zhao, J.; Ma, W.; 526 Yan, H. Donor Polymer Design Enables Efficient Non-Fullerene
- 527 Organic Solar Cells. Nat. Commun. 2016, 7, 13094.
 528 (23) Parr, R. G. Density Functional Theory of Atoms and Molecules.
- 529 Horizons of Quantum Chemistry: Proceedings of the Third International 530 Congress of Quantum Chemistry; Springer: Kyoto, Japan, 1980; pp 5–531 15.
- 532 (24) Becke, A. D. Density-Functional Thermochemistry. III. The 533 Role of Exact Exchange. *J. Chem. Phys.* **1993**, *98*, 5648–5652.
- 534 (25) Runge, E.; Gross, E. K. U. Density-Functional Theory for Time-535 Dependent Systems. *Phys. Rev. Lett.* **1984**, *52*, 997.
- 536 (26) Adamo, C.; Jacquemin, D. The Calculations of Excited-State 537 Properties with Time-Dependent Density Functional Theory. *Chem.* 538 Soc. Rev. **2013**, 42, 845.
- 539 (27) Brause, R.; Krügler, D.; Schmitt, M.; Kleinermanns, K.; 540 Nakajima, A.; Miller, T. A. Determination of the Excited-State
- 541 Structure of 7-Azaindole-Water Cluster using a Franck-Condon
- 542 Analysis. J. Chem. Phys. 2005, 123, 224311.
- 543 (28) Hlel, A.; Mabrouk, A.; Chemek, M.; Khalifa, I. B.; Alimi, K. A 544 DFT Study of Charge-Transfer and Opto-Electronic Properties of
- 545 Some New Materials Involving Carbazole Units. *Comput. Condens.* 546 *Matter* **2015**, 3, 30–40.
- 547 (29) Sen, C. P.; Valiyaveettil, S. Synthesis and Structure-Property 548 Investigation of Multi-Arm Oligothiophenes. *RSC Adv.* **2015**, *5*, 549 105435—105445
- 550 (30) Frisch, M. J.; Trucks, G. W.; Schlegel, H. B.; Scuseria, G. E.; 551 Robb, M. A.; Cheeseman, J. R.; Scalmani, G.; Barone, V.; Petersson, G.
- 552 A.; Nakatsuji, H.; et al. *Gaussian 09*, Revision B.01; Gaussian, Inc.: 553 Wallingford CT, 2016.
- 555 (31) Yanai, T.; Tew, D. P.; Handy, N. C. A New Hybrid Exchange— 555 Correlation Functional Using the Coulomb-Attenuating Method
- 555 Correlation Functional Using the Coulomb-Attenuating Method 556 (CAM-B3LYP). *Chem. Phys. Lett.* **2004**, 393, 51–57. 557 (32) Bouzzine, S. M.; Salgado-Morán, G.; Hamidi, M.; Bouachrine,
- 558 M.; Pacheco, A. G.; Glossman-Mitnik, D. DFT Study on 559 Polythiophene Energy Band Gap and Substitution Effects. *J. Chem.* 560 **2015**, 2015, 1–12.
- 561 (33) Bouman, M. M.; Havinga, E. E.; Janssen, R. A. J.; Meijer, E. W. 562 Chiroptical Properties of Regioregular Chiral Polythiophenes. *Mol.* 563 *Cryst. Liq. Cryst. Sci. Technol., Sect. A* 1994, 256, 439–448.
- 564 (34) Martin, T. P.; Wise, A. J.; Busby, E.; Gao, J.; Roehling, J. D.; 565 Ford, M. J.; Larsen, D. S.; Moulé, A. J.; Grey, J. K. Packing Dependent 566 Electronic Coupling in Single Poly(3-hexylthiophene) H- and J-
- 567 Aggregate Nanofibers. J. Phys. Chem. B 2013, 117, 4478–4487.
- 568 (35) Spano, F. C. The Spectral Signatures of Frenkel Polarons in H-569 and J-Aggregates. *Acc. Chem. Res.* **2010**, *43*, 429–439.
- 570 (36) van Stokkum, I. H. M.; Larsen, D. S.; van Grondelle, R. Global 571 and Target Analysis of Time-Resolved Spectra. *Biochim. Biophys. Acta*, 572 *Bioenerg.* **2004**, *1657*, 82–104.
- 573 (37) Batista, E. R.; Martin, R. L. Exciton Localization in a Pt-574 Acetylide Complex. J. Phys. Chem. A 2005, 109, 9856–9859.
- 575 (38) Schwartz, B. J.; Nguyen, T.-Q.; Wu, J.; Tolbert, S. H. Interchain 576 and Intrachain Exciton Transport in Conjugated Polymers: Ultrafast 577 Studies of Energy Migration in Aligned MEH-PPV/mesoporous Silica 578 Composites. *Synth. Met.* **2001**, *116*, 35–40.
- 579 (39) Westenhoff, S.; Beenken, W. J. D.; Friend, R. H.; Greenham, N. 580 C.; Yartsev, A.; Sundström, V. Anomalous Energy Transfer Dynamics 581 due to Torsional Relaxation in a Conjugated Polymer. *Phys. Rev. Lett.* 582 **2006**, *97*, 166804.
- 583 (40) Guo, J.; Ohkita, H.; Benten, H.; Ito, S. Near-IR Femtosecond 584 Transient Absorption Spectroscopy of Ultrafast Polaron and Triplet 585 Exciton Formation in Polythiophene Films with Different Regior-586 egularities. *J. Am. Chem. Soc.* **2009**, *131*, 16869–16880.

- (41) Szarko, J. M.; Rolczynski, B. S.; Lou, S. J.; Xu, T.; Strzalka, J.; 887 Marks, T. J.; Yu, L.; Chen, L. X. Photovoltaic Function and Exciton/ 588 Charge Transfer Dynamics in a Highly Efficient Semiconducting 589 Copolymer. *Adv. Funct. Mater.* **2014**, 24, 10–26.
- (42) Kraus, H.; Heiber, M. C.; Väth, S.; Kern, J.; Deibel, C.; Sperlich, 591 A.; Dyakonov, V. Analysis of Triplet Exciton Loss Pathways in 592 PTB7:PC71BM Bulk Heterojunction Solar Cells. *Sci. Rep.* **2016**, *6*, 593 29158.
- (43) Ohkita, H.; Cook, S.; Astuti, Y.; Duffy, W.; Heeney, M.; 595 Tierney, S.; McCulloch, I.; Bradley, D. D. C.; Durrant, J. R. Radical Ion 596 Pair Mediated Triplet Formation in Polymer-Fullerene Blend Films. 597 Chem. Commun. 2006, 3939–3941.
- (44) Chow, P. C. Y.; Gélinas, S.; Rao, A.; Friend, R. H. Quantitative 599 Bimolecular Recombination in Organic Photovoltaics through Triplet 600 Exciton Formation. *J. Am. Chem. Soc.* **2014**, *136*, 3424–3429.
- (45) Lee, C.; Yang, W.; Parr, R. G. Development of the Colle-Salvetti 602 Correlation-Energy Formula Into a Functional of the Electron Density. 603 Phys. Rev. B: Condens. Matter Mater. Phys. 1988, 37, 785. 604
- (46) Zhang, A.; Xiao, C.; Wu, Y.; Li, Ć.; Ji, Y.; Li, L.; Hu, W.; Wang, 605 Z.; Ma, W.; Li, W. Effect of Fluorination on Molecular Orientation of 606 Conjugated Polymers in High Performance Field-Effect Transistors. 607 *Macromolecules* **2016**, 49, 6431.
- (47) Bredas, J.; Heeger, A. Theoretical Investigation of Gas-Phase 609 Torsion Potentials along Conjugated Polymer Backbones: Polyacety- 610 lene, Polydiacetylene, and Polythiophene. *Macromolecules* **1990**, 23, 611 1150.
- (48) Meager, I.; Ashraf, R. S.; Mollinger, S.; Schroeder, B. C.; 613 Bronstein, H.; Beatrup, D.; Vezie, M. S.; Kirchartz, T.; Salleo, A.; 614 Nelson, J.; et al. Photocurrent Enhancement from Diketopyrrolopyr- 615 role Polymer Solar Cells through Alkyl-Chain Branching Point 616 Manipulation. *J. Am. Chem. Soc.* 2013, 135, 11537–11540.
- (49) Zhang, F.; Hu, Y.; Schuettfort, T.; Di, C.-a.; Gao, X.; McNeill, C. 618 R.; Thomsen, L.; Mannsfeld, S. C. B.; Yuan, W.; Sirringhaus, H.; et al. 619 Critical Role of Alkyl Chain Branching of Organic Semiconductors in 620 Enabling Solution-Processed N-Channel Organic Thin-Film Tran- 621 sistors with Mobility of up to 3.50 cm(2) V-1 s(-1). *J. Am. Chem. Soc.* 622 **2013**, 135, 2338–2349.